

Magnetic polarizability of a charged pion from four-point functions in lattice QCD

Frank X. Lee,^{1,*} Walter Wilcox,^{2,†} Andrei Alexandru,^{1,3,‡} and Chris Culver^{4,§}

¹*Physics Department, The George Washington University, Washington, DC 20052, USA*

²*Department of Physics, Baylor University, Waco, Texas 76798, USA*

³*Department of Physics, University of Maryland, College Park, MD 20742, USA*

⁴*Department of Mathematical Sciences, University of Liverpool, Liverpool L69 7ZL, United Kingdom*

Electromagnetic dipole polarizabilities are fundamental properties of a hadron that represent its resistance to deformation under external fields. For a charged hadron, the presence of acceleration and Landau levels complicates the isolation of its deformation energy in the conventional background field method. In this work, we explore a general method based on four-point functions in lattice QCD that takes into account all photon, quark and gluon interactions. The electric polarizability (α_E) has been determined from the method in a previous proof-of-principle simulation. Here we focus on the magnetic polarizability (β_M) using the same quenched Wilson action on a $24^3 \times 48$ lattice at $\beta = 6.0$ with pion mass from 1100 to 370 MeV. The results from the connected diagrams show a large cancellation between the elastic and inelastic contributions, leading to a relatively small and negative value for β_M consistent with chiral perturbation theory. We also discuss the mechanism for $\alpha_E + \beta_M$ from combining the two studies.

I. INTRODUCTION

Understanding electromagnetic polarizabilities has been a long-term goal of lattice QCD. The standard approach is the background field method which introduces classical static electromagnetic fields to interact with quarks in QCD [1–32]. The appeal of the method lies in its simplicity: only two-point correlation functions are needed to measure the small energy shift with or without the external field, which amounts to a standard calculation of a hadron’s mass. The energy shift linear in the applied field is related to dipole moments, and the quadratic shift to polarizabilities. The method is fairly robust and has been widely applied to neutral hadrons.

When it comes to charged hadrons, however, the method is faced with new challenges. The reason is rather rudimentary: a charged particle accelerates in an electric field and exhibits Landau levels in a magnetic field. Such collective motion of the hadron is unrelated to moments and polarizabilities and must be disentangled from the total energy shift in order to isolate the deformation energy on which the polarizabilities are defined. The traditional method of extracting ground state energy at large times breaks down since the two-point function no longer has a single-exponential behavior. Special techniques have to be developed to analyze such functions. Nonetheless, progress has been made. For electric field, a continuum relativistic propagator for a charged scalar is used to demonstrate how to fit such lattice data for charged pions and kaons [10, 11]. It is improved upon by an effective propagator exactly matching the lattice being used to generate the lattice QCD data [32]. Furthermore, spatial and time profiles $G(x, t)$ under Dirichlet boundary conditions

with both real and imaginary parts are used to capture the interactions while maintaining gauge invariance in the background field. For magnetic field, various techniques have been tried to deal with Landau levels, from direct fitting forms [18–23], to formal studies of Dirac operator [24, 25], to a novel Laplacian-mode projection technique at the quark propagator level [27–31].

Here we advocate an alternative approach based on four-point functions in lattice QCD. Instead of background fields, electromagnetic currents couple to quark fields. All photon-quark, quark-quark, and gluon-quark interactions are included. It is a general approach that treats neutral and charged particles on equal footing. The potential of using four-point functions to access polarizabilities has been investigated in the early days of lattice QCD [33–35]. The effort was deemed too computationally demanding at the time and the results on limited lattices were inconclusive. Recently, there is a renewed interest to revive such efforts, partly spurred by the challenges encountered in the background field method for charged particles. A reexamination of the formalism in Ref. [35] is carried out in Ref. [36] in which new formulas are derived in momentum space for electric and magnetic polarizabilities of both charged pion and proton. It is followed by a proof-of-principle simulation for the electric polarizability of a charged pion [37]. In this work, we extend the calculation to magnetic polarizability using the same lattice parameters. We note there exists other four-point function calculations on polarizabilities. Ref. [38] employs a position-space formula for the Compton tensor to calculate charge pion electric polarizability near the physical point, along with a preliminary calculation on the proton [39]. A comprehensive review on pion polarizabilities from other theoretical approaches and experiment can be found in Ref. [40, 41]. We also note that although Refs. [8, 42] are based on the background field method, they are in fact four-point function calculations. A perturbative expansion in the background field at the action level is performed in which two vector current insertions

* fxlee@gwu.edu

† walter_wilcox@baylor.edu

‡ aalexan@gwu.edu

§ c.culver@liverpool.ac.uk

couple the background field to the hadron correlation function, leading to the same diagrammatic structures as in this work.

In Sec. II we outline the methodology to extract magnetic polarizability of a charged pion from four-point functions. In Sec. III we show our results from a proof-of-concept simulation. In particular, we discuss β_M and its chiral extrapolation, $\alpha_E + \beta_M$, and comparison with ChPT. In Sec. IV we give concluding remarks. The four-point correlation functions needed in the simulation are given in the Appendix.

II. METHODOLOGY

In Ref. [36], a formula is derived for electric polarizability of a charged pion,

$$\alpha_E = \frac{\alpha \langle r_E^2 \rangle}{3m_\pi} + \lim_{q \rightarrow 0} \frac{2\alpha}{q^2} \int_0^\infty dt \left[Q_{44}(\mathbf{q}, t) - Q_{44}^{elas}(\mathbf{q}, t) \right], \quad (1)$$

and for its magnetic polarizability,

$$\beta_M = -\frac{\alpha \langle r_E^2 \rangle}{3m_\pi} + \lim_{q \rightarrow 0} \frac{2\alpha}{q^2} \int_0^\infty dt \left[Q_{11}^{inel}(\mathbf{q}, t) - Q_{11}^{inel}(\mathbf{0}, t) \right]. \quad (2)$$

Here $\alpha = 1/137$ is the fine structure constant. The formulas are in discrete Euclidean spacetime but we keep the time axis continuous for notational convenience. Zero-momentum Breit frame is employed in the formula to mimic low-energy Compton scattering, where the initial and final pions are at rest and the photons have purely spacelike momentum. The formulas have a similar structure in that they both have an elastic contribution in terms of the charge radius and pion mass, and an inelastic contribution in the form of subtracted time integrals. They differ in two aspects. The Q_{44} in α_E includes both elastic and inelastic contributions whereas the Q_{11}^{inel} in β_M includes only inelastic contributions. In α_E , the elastic $Q_{44}^{elas}(\mathbf{q}, t)$ is subtracted, whereas in β_M it is the zero-momentum inelastic $Q_{11}^{inel}(\mathbf{0}, t)$ that is subtracted.

Both α_E and β_M have the expected physical unit of a^3 (fm^3). In the elastic term $\langle r_E^2 \rangle$ scales like a^2 and m_π like a^{-1} . In the inelastic term $1/q^2$ scales like a^2 , t scales like a , and Q_{44} and Q_{11} are dimensionless by definition. The α_E has been studied thoroughly in a previous work [37], from which we take the results for pion mass m_π and charge radius $\langle r_E^2 \rangle$ and α_E . In this work we focus on the β_M in Eq. (2).

The four-point function Q_{11} is defined as,

$$Q_{11}(\mathbf{q}, t_3, t_2, t_1, t_0) \equiv \frac{\sum_{\mathbf{x}_3, \mathbf{x}_2, \mathbf{x}_1, \mathbf{x}_0} e^{-i\mathbf{q} \cdot \mathbf{x}_2} e^{i\mathbf{q} \cdot \mathbf{x}_1} \langle \Omega | \psi(\mathbf{x}_3) : j_1^L(\mathbf{x}_2) j_1^L(\mathbf{x}_1) : \psi^\dagger(\mathbf{x}_0) | \Omega \rangle}{\sum_{\mathbf{x}_3, \mathbf{x}_0} \langle \Omega | \psi(\mathbf{x}_3) \psi^\dagger(\mathbf{x}_0) | \Omega \rangle}. \quad (3)$$

In this expression, Ω denotes the vacuum, and normal ordering is used to include the required subtraction of

vacuum expectation values (VEV) on the lattice. The sums over \mathbf{x}_0 and \mathbf{x}_3 enforce zero-momentum pions at the source (t_0) and sink (t_3). The sum over \mathbf{x}_1 injects momentum \mathbf{q} by the current at t_1 , whereas sum over \mathbf{x}_2 takes out \mathbf{q} by the current at t_2 to satisfy energy-momentum conservation in the process. The two possibilities of time ordering are implied in the normal ordering. The time t in Eq.(1) and Eq.(2) represents the separation between the two currents $t = t_2 - t_1$ with the two fixed ends t_0 and t_3 implied.

We consider π^+ with standard interpolating field,

$$\psi_{\pi^+}(x) = \bar{d}(x)\gamma_5 u(x), \quad (4)$$

For the lattice version of electromagnetic current density in the x -direction, we consider two options. One is a local current (or point current) built from up and down quark fields,

$$j_1^{(PC)} \equiv i Z_V \kappa (q_u \bar{u} \gamma_1 u + q_d \bar{d} \gamma_1 d). \quad (5)$$

The factor i here is needed to ensure that the spatial component $j_1^{(PC)}$ is hermitian, in contrast to the time component $j_4^{(PC)}$ in the electric case [37]. The reason is $(\bar{u} \gamma_1 u)^\dagger = -\bar{u} \gamma_1 u$ whereas $(\bar{u} \gamma_4 u)^\dagger = \bar{u} \gamma_4 u$ (recall $\bar{u} \equiv u^\dagger \gamma_4$). The factor κ is to account for the quark-field rescaling $\psi \rightarrow \sqrt{2\kappa} \psi$ in Wilson fermions. The factor 2 is canceled by the $1/2$ factor in the definition of the vector current $\frac{1}{2} \bar{\psi} \gamma_\mu \psi$. The charge factors are $q_u = 2/3$ and $q_d = -1/3$ where the resulting $e^2 = \alpha$ in the four-point function has been absorbed in the definition of β_M in Eq.(2). The advantage of this operator is that it leads to simple correlation functions. The drawback is that the renormalization constant for the vector current has to be determined. The other option is the conserved vector current for Wilson fermions on the lattice ($Z_V \equiv 1$) in point-split form,

$$j_1^{(PS)}(x) \equiv i q_u \kappa_u \left[-\bar{u}(x)(1 - \gamma_\mu)U_1(x)u(x + \hat{1}) + \bar{u}(x + \hat{\mu})(1 + \gamma_1)U_1^\dagger(x)u(x) \right] + i q_d \kappa_d \left[-\bar{d}(x)(1 - \gamma_1)U_1(x)d(x + \hat{1}) + \bar{d}(x + \hat{1})(1 + \gamma_1)U_1^\dagger(x)d(x) \right]. \quad (6)$$

Although conserved current explicitly involves gauge fields and lead to more complicated correlation functions, it has the advantage of circumventing the renormalization issue. All results in this work are based on conserved current.

At the quark level, Wick contractions of quark-antiquark pairs in Q_{11} in Eq.(3) lead to topologically distinct quark-line diagrams shown in Fig. 1. We focus on the connected contributions in this study. The total connected contribution is simply the sum of the individual normalized terms,

$$Q_{11}(\mathbf{q}, t_2, t_1) = Q_{11}^{(a)} + Q_{11}^{(b)} + Q_{11}^{(c)}, \quad (7)$$

for either point current or conserved current. The charge factors and flavor-equivalent contributions have been included in each diagram. The disconnected contributions are more challenging and are left for future work.

III. SIMULATION DETAILS AND RESULTS

We use quenched Wilson action with $\beta = 6.0$ and $\kappa = 0.1520, 0.1543, 0.1555, 0.1565$ on the lattice $24^3 \times 48$. We analyzed 500 configurations for $\kappa = 0.1520$ and 1000 configurations each for rests of the kappas. The scale of this action has been determined in Ref. [43], with inverse lattice spacing $1/a = 2.312$ GeV and kappa critical $\kappa_c = 0.15708$. Dirichlet (or open) boundary condition is imposed in the time direction, while periodic boundary conditions are used in spatial dimensions. The pion source is placed at $t_0 = 7$ and sink at $t_3 = 42$ (time is labeled from 1 to 48). One current is inserted at a fixed time t_1 , while the other current t_2 is free to vary. We consider four different combinations of momentum $\mathbf{q} = \{0, 0, 0\}, \{0, 0, 1\}, \{0, 1, 1\}, \{0, 0, 2\}$. In lattice units they correspond to the values $\mathbf{q}^2 a^2 = 0, 0.068, 0.137, 0.274$, or in physical units to $\mathbf{q}^2 = 0, 0.366, 0.733, 1.465$ (GeV²).

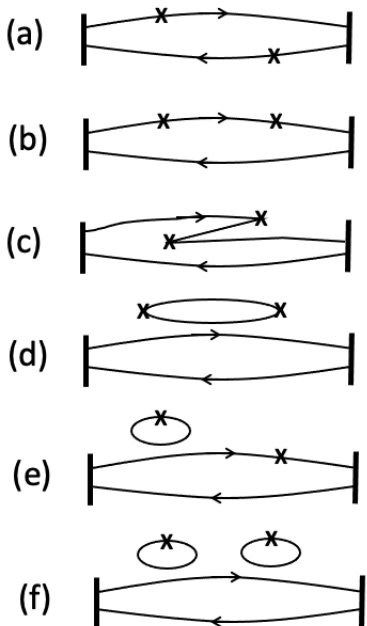


FIG. 1. Quark-line diagrams of a four-point function contributing to polarizabilities of a charged pion. Diagrams a,b,c are connected contributions whereas diagrams d,e,f are disconnected contributions. In each diagram, flavor permutations are assumed as well as gluon lines that connect the quark lines. The zero-momentum pion interpolating fields are represented by vertical bars (wall sources).

A. Raw correlation functions

In Fig. 2 we show the raw normalized four-point functions, both individually and collectively, at the four different values of momentum \mathbf{q} and at $m_\pi = 600$ MeV. All points are included and displayed on a linear scale for comparison purposes. The special point of $t_1 = t_2$ is regular in diagram a, but gives irregular results in diagram b and c at all values of \mathbf{q} . The same irregularity is observed in the electric case. It is an unphysical contact interaction on the lattice which vanishes in the continuum limit. We treat this point with special care in our analysis below. The results about $t_1 = 18$ in diagram b and c are mirror images of each other, simply due to the fact that they are from the two different time orderings of the same diagram. In principle, this property could be exploited to reduce the cost of simulations by placing t_1 in the center of the lattice. In this study, however, we computed all three diagrams separately, and add them between $t_1 = 19$ and $t_3 = 41$ as the signal.

To see the structure of the four-point function in Eq.(3), we insert a complete set of intermediate states in the numerator (trice) and in the denominator (once), and make use of translation invariance and kinematics,

$$\begin{aligned}
 Q_{11}(\mathbf{q}, t_3, t_2, t_1, t_0) &= \sum_{\mathbf{x}_3, \mathbf{x}_2, \mathbf{x}_1, \mathbf{x}_0} N_s^3 \sum_{n, n_i, n_f} \\
 &\langle \Omega | \psi(\mathbf{0}) | n_f(\mathbf{0}) \rangle e^{-am_\pi(t_3-t_2)} \\
 &\langle n_f(\mathbf{0}) | j_1^L(0) | n(\mathbf{q}) \rangle e^{-aE_n(\mathbf{q})(t_2-t_1)} \\
 &\langle n(\mathbf{q}) | j_1^L(0) | n_i(\mathbf{0}) \rangle e^{-am_\pi(t_1-t_0)} \langle n_i(\mathbf{0}) | \psi^\dagger(\mathbf{0}) | \Omega \rangle \\
 &/ [\sum_{\mathbf{x}_3, \mathbf{x}_0} N_s \sum_n \langle \Omega | \psi(\mathbf{0}) | n(\mathbf{0}) \rangle e^{-am_n(t_3-t_0)} \langle n(\mathbf{0}) | \psi^\dagger(\mathbf{0}) | \Omega \rangle] \quad (8) \\
 &- N_s \sum_n \langle \Omega | j_1^L(0) | n(\mathbf{q}) \rangle e^{-aE_n(\mathbf{q})(t_2-t_1)} \langle n(\mathbf{q}) | j_1^L(0) | \Omega \rangle \\
 &= -N_s^2 |\langle \pi(\mathbf{0}) | j_1^L(0) | \pi(\mathbf{q}) \rangle|^2 e^{-a(E_\pi - m_\pi)(t_2-t_1)} \\
 &\quad + N_s |\langle \Omega | j_1^L(0) | \pi(\mathbf{q}) \rangle|^2 e^{-aE_\pi(t_2-t_1)} + \dots,
 \end{aligned}$$

where the leading contributions are isolated in the last step under time limits $t_3 \gg t_{1,2} \gg t_0$. The change of sign is due to the metric factor for spatial components in Eq.(5). The $N_s = N_x N_y N_z$ is the number of spatial sites on the lattice. The normal ordering in Eq.(3) is formally defined as,

$$\begin{aligned}
 &\langle \Omega | \psi(x_3) : j_1^L(x_2) j_1^L(x_1) : \psi^\dagger(x_0) | \Omega \rangle \\
 &\equiv \langle \Omega | \psi(x_3) T [j_1^L(x_2) j_1^L(x_1)] \psi^\dagger(x_0) | \Omega \rangle \quad (9) \\
 &- \langle \Omega | T j_1^L(x_2) j_1^L(x_1) | \Omega \rangle \langle \Omega | \psi(x_3) \psi^\dagger(x_0) | \Omega \rangle,
 \end{aligned}$$

where T in the first term means time-ordering and the second term signifies a subtraction of vacuum expectation values (VEV) on the lattice in the disconnected diagrams. In fact, subtraction is only needed for diagram d; it vanishes for diagrams e and f. The pion two-point function cancels exactly in the second term in Eq.(8).

Poin form factor is contained in the elastic matrix

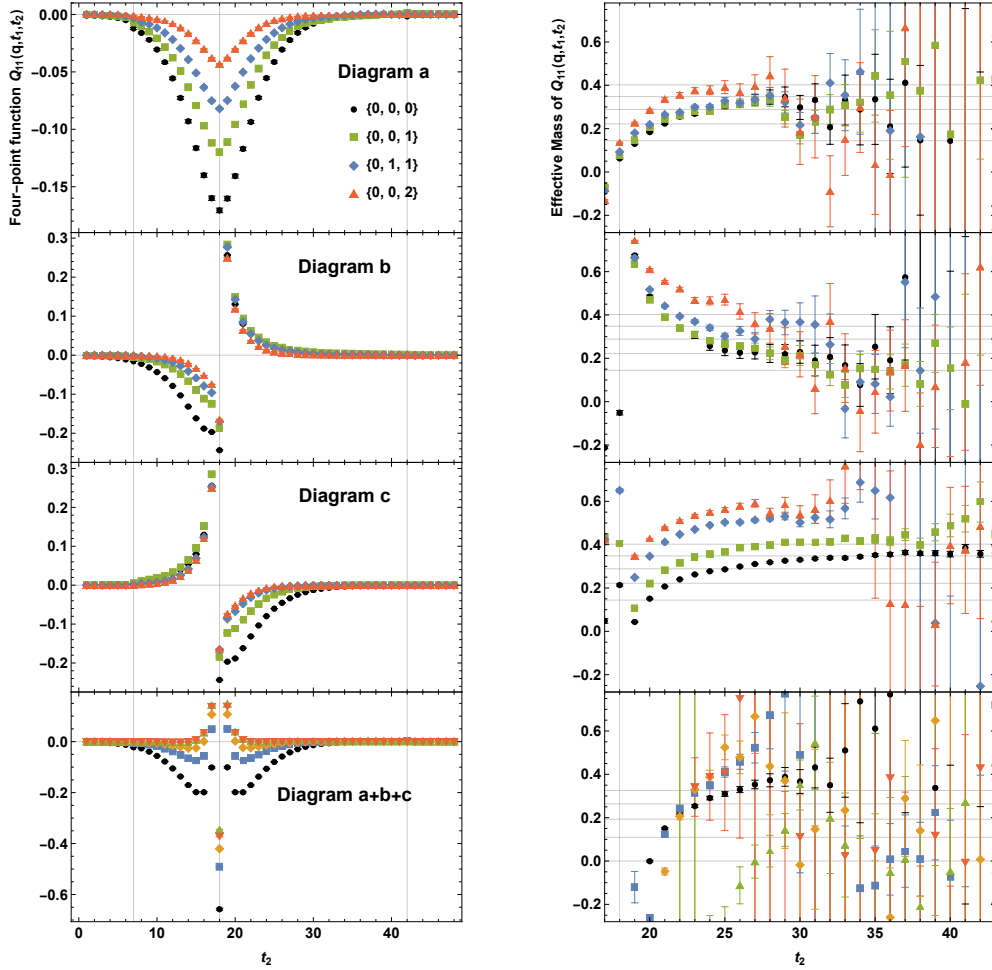


FIG. 2. Individual and total four-point functions (left) and their effective mass functions (right) from the connected diagrams as a function of current separation at $m_\pi = 600$ MeV. Vertical gridlines indicate the pion walls ($t_0 = 7$ and $t_3 = 42$) and the fixed current insertion ($t_1 = 18$). Horizontal gridlines in the effective mass functions are $E_\rho - m_\pi$ in lattice units where $E_\rho = \sqrt{\mathbf{q}^2 + m_\rho^2}$ with measured m_π and m_ρ . The results in the total between $t_2 = 19$ and $t_2 = 41$ will be the signal for our analysis.

element,

$$\begin{aligned} & \langle \pi(p') | j_\mu^L(0) | \pi(p) \rangle \\ & = (p' + p)_\mu F_\pi(q^2) + q_\mu \frac{p'^2 - p^2}{q^2} (1 - F_\pi(q^2)). \end{aligned} \quad (10)$$

It vanishes for j_1^L as long as $(p' + p)_\mu$ does not have a $\mu = 1$ component. The condition is indeed satisfied under the zero-momentum Breit frame and our selection of \mathbf{q} values. This is the reason that $\mathbf{q} = \{1, 1, 1\}$ is excluded from the set of \mathbf{q} values relative to the electric case.

In other words, there is no elastic contribution in the second term of β_M in Eq.(2) as long as transverse momentum to j_1^L is considered. This is evident in the effective mass functions in Fig. 2 where the intermediate states are not on-shell pions, but states with different mass and energy. Possible intermediate states are either vector

or axial mesons in the magnetic channel. For reference, we draw horizontal lines $E_\rho - m_\pi$ in lattice units where $E_\rho = \sqrt{\mathbf{q}^2 + m_\rho^2}$, using measured m_π and m_ρ . The effective mass functions in Fig. 2 are only provided for reference purposes on the intermediate state. They can become noisy at large current separations and higher momentum. This is not a concern since there is no fitting performed at large times. The signal is the time integral of subtracted four-point functions, which amounts to evaluating the area between two curves. And the signal is dominant at small times.

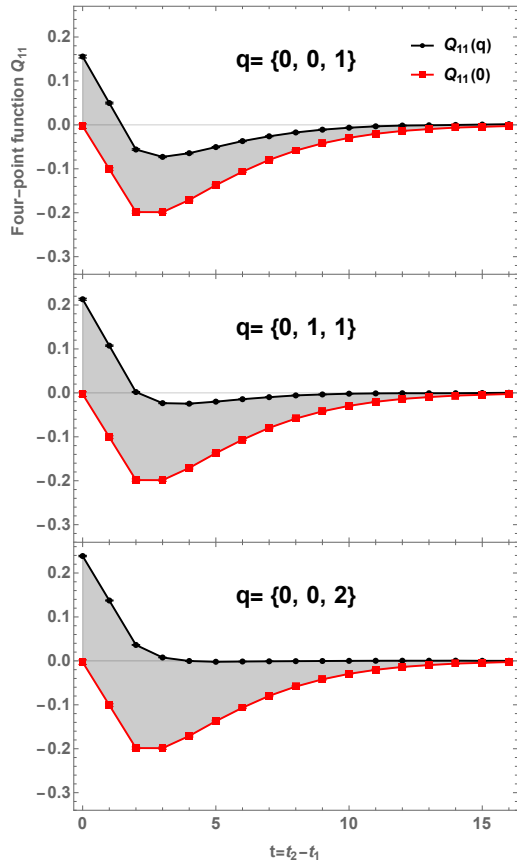


FIG. 3. Momentum-carrying $Q_{11}(\mathbf{q})$ and zero-momentum $Q_{11}(\mathbf{0})$ at different values of \mathbf{q} at $m_\pi = 600$ MeV. The shaded area between the two is the dimensionless signal contributing to magnetic polarizability.

B. Magnetic polarizability

In Fig. 3 we show the connected contribution $Q_{11}(\mathbf{q})$ at different \mathbf{q} values and zero-momentum $Q_{11}(\mathbf{0})$ as a function of current separation $t = t_2 - t_1$ in lattice units. Only results for $m_\pi = 600$ MeV are shown as an example; the graphs at the other pion masses look similar. The time integral required for β_M in the formula, $(1/a) \int dt [Q_{11}(\mathbf{q}, t) - Q_{11}(\mathbf{0}, t)]$, is simply the shaded area between the two curves, and it is positive. One detail to notice is that the curves include the $t = 0$ point which has unphysical contributions in Q_{11} mentioned earlier. We would normally avoid this point and only start the integral from $t = 1$. However, the chunk of area between $t = 0$ and $t = 1$ is the largest piece in the integral. To include this contribution, we linearly extrapolated both $Q_{11}(\mathbf{q})$ and $Q_{11}(\mathbf{0})$ back to $t = 0$ using the two points at $t = 1$ and $t = 2$. As the continuum limit is approached, the $t = 0$ point will become regular and the chunk will shrink to zero.

The inelastic term can now be constructed by multiplying $2\alpha/\mathbf{q}^2$ and the time integral, and it is a function of momentum. Since β_M is a static property, we extrapolate it to $\mathbf{q}^2 = 0$ smoothly. We consider two fits, a quadratic fit $a + bx + cx^2$ ($x = \mathbf{q}^2$) using all three data points, and a linear fit using the two lowest points. The results are shown in Fig. 4 for all pion masses. One observes a spread in the extrapolated values at $\mathbf{q}^2 = 0$. We treat the spread as a systematic effect as follows. We take the average of the two extrapolated values along with statistical uncertainties, and half of the difference in their central values as a systematic uncertainty. The statistical and systematic uncertainties are then propagated in quadrature to the analysis of β_M . For our data, the statistical uncertainties are relatively small, so the systematic uncertainties are dominant in the inelastic contribution.

Finally, we assemble the two terms in the formula

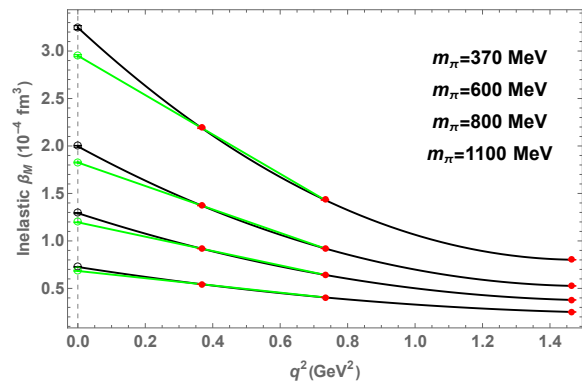


FIG. 4. Momentum dependence of the inelastic term in Eq. (2) and its extrapolation to $\mathbf{q}^2 = 0$ at all pion masses. Red points are based on the shaded areas in Fig. 3. Black curve is a quadratic extrapolation using all three points. Green curve is a linear extrapolation based on the two lowest points. Empty points indicate the corresponding extrapolated values contributing to β_M .

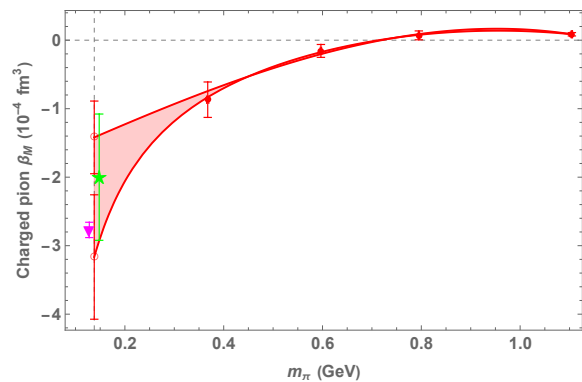


FIG. 5. Chiral extrapolation of charged pion magnetic polarizability. For better viewing, the PDG value (star) and ChPT value (triangle) are shifted horizontally by 10 MeV.

TABLE I. Summary of results in physical units from two-point and four-point functions. Results for charge radius and α_E are taken from previous work [37]. Elastic β_M and total β_M are chirally extrapolated to the physical point. Inelastic β_M at the physical point is taken as the difference of the two. Known values from ChPT and PDG are listed for reference. All polarizabilities are in units of 10^{-4} fm^3 .

	$\kappa=0.1520$	$\kappa=0.1543$	$\kappa=0.1555$	$\kappa=0.1565$	physical point	known value
m_π (MeV)	1104.7 ± 1.2	795.0 ± 1.1	596.8 ± 1.4	367.7 ± 2.2	138	138
m_ρ (MeV)	1273.1 ± 2.5	1047.3 ± 3.4	$930. \pm 7.$	$830. \pm 17.$	770	770
$\langle r_E^2 \rangle$ (fm ²)	0.1424 ± 0.0029	0.195 ± 0.007	0.257 ± 0.005	0.304 ± 0.016	0.40 ± 0.05	0.434 ± 0.005 (PDG)
α_E elastic	0.618 ± 0.012	1.17 ± 0.04	2.07 ± 0.04	3.97 ± 0.21	13.9 ± 1.8	15.08 ± 0.13 (PDG)
α_E inelastic	-0.299 ± 0.019	-0.672 ± 0.030	-0.92 ± 0.11	-1.27 ± 0.13	-9.7 ± 1.9 to -5.1 ± 2.0	
α_E total	0.319 ± 0.023	0.50 ± 0.05	1.15 ± 0.11	2.70 ± 0.25	4.2 ± 0.5 to 8.8 ± 0.9	2.93 ± 0.05 (ChPT) $2.0 \pm 0.6 \pm 0.7$ (PDG)
β_M elastic	-0.618 ± 0.012	-1.17 ± 0.04	-2.07 ± 0.04	-3.97 ± 0.21	-13.9 ± 1.8	-15.08 ± 0.13 (PDG)
β_M inelastic	0.705 ± 0.021	1.24 ± 0.05	1.91 ± 0.09	3.10 ± 0.15	10.7 ± 2.0 to 12.4 ± 1.9	
β_M total	0.087 ± 0.024	0.07 ± 0.06	-0.16 ± 0.09	-0.87 ± 0.26	-3.2 ± 0.9 to -1.4 ± 0.5	-2.77 ± 0.11 (ChPT) $-2.0 \pm 0.6 \pm 0.7$ (PDG)

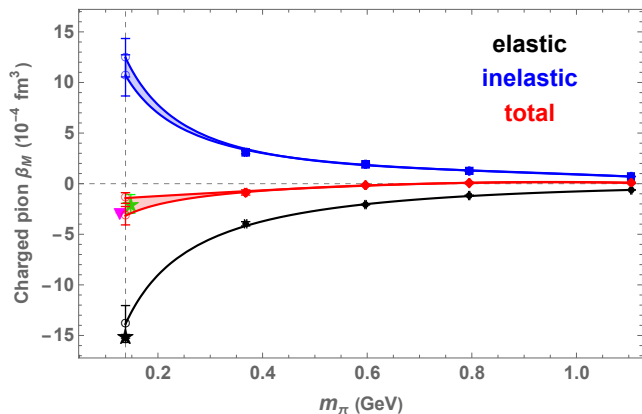


FIG. 6. Individual and total contributions to charged pion β_M from four-point functions in lattice QCD based on the formula in Eq.(2). The total is taken from Fig. 5, and the elastic from Ref. [37]; both are chirally extrapolated to the physical point. The inelastic is from the difference of the two.

in Eq.(2) to obtain β_M in physical units. The results are summarized in Fig. 5 and in Table I. At each pion mass the elastic term is negative, whereas the inelastic term is positive. The total is slightly positive at the two heaviest pion masses, then turns negative as the pion mass is lowered. To see how the trend continues to smaller pion masses, we take the total values for β_M at the four pion masses and perform a smooth extrapolation to the physical point. Since our pion masses are relatively large, we consider two forms to cover the range of uncertainties in the extrapolation: a polynomial form $a + b m_\pi + c m_\pi^3$ and a form with a divergent $1/m_\pi$ term $\frac{a}{m_\pi} + b m_\pi + c m_\pi^3$ inspired by ChPT [44, 45]. The spread can be considered as a systematic effect. The extrapolated value of -3.2 ± 0.9 to -1.4 ± 0.5 at the physical point is comparable to the known value of $-2.0 \pm 0.6 \pm 0.7$ from PDG [46] and

$-2.77(11)$ from two-loop contribution of ChPT [41, 44]. An interesting feature is a sign change from positive to negative as pion mass is lowered. It happens around 750 MeV. In contrast, there is no sign change in the electric case.

To get an overview on how the β_M comes about, we show in Fig. 6 three terms on the same graph: elastic, inelastic, and their sum. The inelastic curve is taken as the difference of the total and the elastic curves. This gives a constraint of 10.7 ± 2.0 to 12.4 ± 1.9 for the inelastic at the physical point. It would be interesting to verify this chiral behavior in the inelastic term directly in future simulations. The results in this figure point to the following physical picture: β_M is the result of a large cancellation between the elastic and inelastic contributions. The cancellation is more significant than in the electric case [37]. This cancellation appears to continue in the approach to the physical point, resulting in a total value that is relatively small and negative, and a relatively mild pion mass dependence compared to the individual contributions. It is almost the complete opposite to the electric case [37].

A comparison on β_M can be made here between the four-point function method and the background field method. For the former, our value of $-3.2(9)$ is the only attempt at the moment. For the latter, there are several calculations. In Ref. [19, 20], β_M is studied for both charged and neutral pions. A fitting form is used that includes Landau levels and up to B^4 contributions in magnetic field for charged pions. Values of $-1.15(31)$ and $-2.06(76)$ are obtained on two different lattices. No chiral extrapolation is performed. Since only bare quark masses are given we could not ascertain what pion masses they correspond to. In Ref. [31], a Laplacian-mode projection technique is employed at the quark propagator level to filter out the Landau levels. The same technique is used on the nucleon [30]. A final value of $-1.70(14)(25)$ is reported. It also predicts a sign change in β_M , but only after chiral

extrapolation. The simulated results are positive at all the pion masses considered, down to about 300 MeV. A Padé form is introduced to extrapolate the positive values to the negative one at the physical point. The sign change happens at around 225 MeV. This is different from the sign change observed in Fig. 6, which happens at a heavier pion mass, before chiral extrapolation. This is an interesting puzzle for future investigations. The resolution could be in the different systematics present in the two calculations. For the four-point function method in this work, it could be the quenched approximation, disconnected diagrams, and the contact term in the connected diagrams.

C. $\alpha_E + \beta_M$

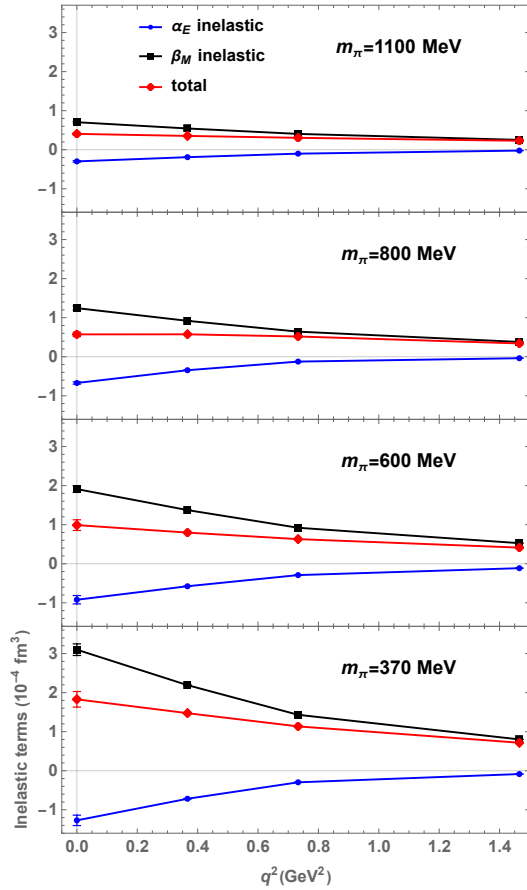


FIG. 7. Momentum dependence of the inelastic terms at different pion masses. The values at $q^2 = 0$ are from a linear extrapolation using the two lowest points. The curves are straight lines connected all the points. The sum of the two inelastic terms (red) is a direct measure of the momentum dependence for $\alpha_E(\mathbf{q}) + \beta_M(\mathbf{q})$.

Here we take a closer look at the sum of electric and magnetic polarizabilities. ChPT gives a solid prediction

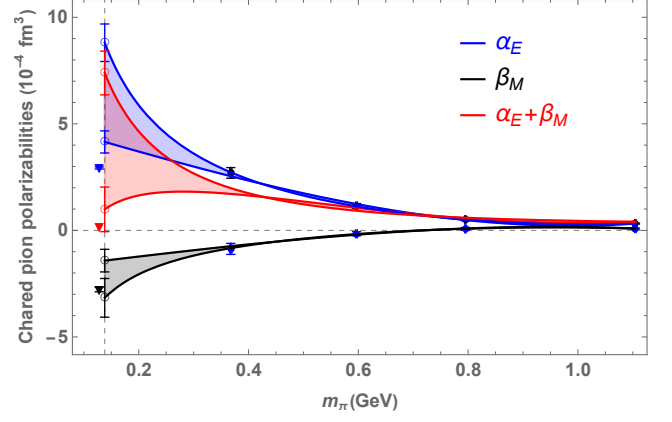


FIG. 8. Pion mass dependence of individual and sum of polarizabilities for a charged pion from four-point functions in lattice QCD. The α_E is previously determined from the formula in Eq.(1) and β_M in the present study from Eq.(2). The curves are nonlinear chiral extrapolations. The color-coded triangles are values from ChPT and they are shifted horizontally by 10 MeV for better viewing.

that $\alpha_E + \beta_M \approx 0$ at leading-order and $\alpha_E + \beta_M \approx 0.16$ at the two-loop order [44] in units of 10^{-4} fm^3 . Baldin sum rule [41, 47] applied to a charged pion gives $\alpha_E + \beta_M \approx 0.39(4)$ in the same units.

In the four-point function formalism, we note first that if we add Eq.(1) and Eq.(2), the elastic charge radius terms cancel exactly, leaving only inelastic contributions in the form of subtracted time integrals,

$$\alpha_E + \beta_M = \lim_{q \rightarrow 0} \frac{2\alpha}{q^2} \int_0^\infty dt \left[Q_{44}(\mathbf{q}, t) - Q_{44}^{elas}(\mathbf{q}, t) + Q_{11}^{inel}(\mathbf{q}, t) - Q_{11}^{inel}(\mathbf{0}, t) \right]. \quad (11)$$

This can be regarded as a sum rule for $\alpha_E + \beta_M$ on the lattice (instead of energy integration over cross sections, it is a time integration over subtracted four-point functions). Second, the inelastic terms are opposite in sign so there is a cancellation in the inelastic contributions as well. Specifically, α_E inelastic is negative whereas β_M inelastic is positive and both are momentum-dependent. In Fig. 7, we show the momentum dependence separately along with their sum including the extrapolated $q^2 = 0$ limit. They are displayed on the same scale at different pion masses to facilitate comparison. The magnetic points are taken from Fig. 4. The electric points are taken from Ref. [37]. Note that we leave out the $\mathbf{q} = \{1, 1, 1\}$ point from the electric case for a one-to-one comparison. The salient feature is that they are not only opposite in sign, but the magnetic is consistently larger than the electric in magnitude, over the entire momentum range. As a result, the cancellation leaves a relatively small and positive value. The value at $q^2 = 0$ appears to grow with decreasing pion mass, which is deviating from ChPT expectations.

Finally, we look at pion mass dependence, by adding

inelastic terms at the $q^2 = 0$ limit and elastic terms. We plot in Fig.8 β_M from this work, α_E from the previous work [37], and their sum on the same graph. We see α_E is positive in the pion mass range studied, and β_M is negative except at the heaviest pion mass of 1100 MeV. The cancellation leads to a positive value for $\alpha_E + \beta_M$ at the three lowest pion masses. It is unclear how the cancellation plays out in the approach to the physical point due to large uncertainties in the extrapolations.

IV. CONCLUSION

Building on the study of electric polarizability α_E for a charged pion using four-point functions in lattice QCD [37], we investigated its magnetic polarizability β_M using the same methodology and simulation parameters. The extension is relatively straightforward, mainly replacing charge-charge correlation (Q_{44}) with current-current correlation (Q_{11}). The formula for β_M in Eq.(2) has a similar structure to the one for α_E in Eq.(1). They share the same charge radius $\langle r_E^2 \rangle$ and pion mass in the elastic contribution, but this term appears with an opposite sign in the two formulas. The inelastic contribution is in the form of a subtracted time integral. In the electric case, it is the elastic $Q_{44}^{elas}(\mathbf{q})$ at each momentum that is subtracted from the total, whereas in the magnetic case it is the zero-momentum inelastic $Q_{11}^{inel}(\mathbf{0})$ that is subtracted. Only Q_{44} is needed for α_E , but both Q_{44} and Q_{11} are needed for β_M due to coupling between the two formulas. The methodology requires two- and four-point functions, but not three-point functions.

The emerging picture in Fig.(6) for β_M is similar to that for α_E , but in the reverse sense: it is the result of a cancellation between a negative elastic contribution and a positive inelastic contribution. The cancellation is more significant than in the electric case. Individually, each contribution has strong pion mass dependence in the approach to the chiral limit, but the total has a small negative value with a relatively mild pion mass dependence. Combining the results of this study and those of Ref. [37], we found that $\alpha_E + \beta_M$ is the consequence of cancellations at three levels to varying degrees. First, there is an exact cancellation in the elastic terms. Second, there is a cancellation in the inelastic terms as a function of momentum, with the magnetic slightly larger than the electric, leaving a relatively weak momentum dependence at fixed pion mass. Third, at the static limit there is a partial cancellation between α_E and β_M at the lowest three pion masses explored, leaving a positive value. Although the resulting sign of $\alpha_E + \beta_M$ is consistent with ChPT, it is unclear quantitatively in the approach to the physical point since chiral extrapolation of the results suffers from large uncertainties. These issues point to the importance of pushing to smaller pion masses.

We caution that the above picture is still subject to a number of systematic effects at the proof-of-principle stage, such as the quenched approximation, finite-volume

effects, and disconnected loops. In particular, there is a systematic effect in the connected diagrams from the contact term when the two currents overlap on the same quark. This is a lattice artifact of unknown size that can only be computed correctly very close to the continuum limit. Additionally, there is a puzzling difference between the four-point function method and the background field method that warrants further study. Although both methods yield similar negative values at the physical point after chiral extrapolation, they have different signs at non-physical pion masses. The resolution should focus on the different systematic effects present in the two studies.

ACKNOWLEDGMENTS

This work was supported in part by U.S. Department of Energy under Grant No. DE-FG02-95ER40907 (FL, AA) and UK Research and Innovation grant MR/S015418/1 (CC). WW would like to acknowledge support from the Baylor College of Arts and Sciences SRA program. AA would like to acknowledge support from University of Maryland. The calculations are carried out at DOE-sponsored NERSC at Livermore and NSF-sponsored TACC at Austin.

-
- [1] Claude Bernard, Terrence Draper, Kirk Olynyk, and Minick Rushton, “Lattice quantum-chromodynamics calculation of some baryon magnetic moments,” *Phys. Rev. Lett.* **49**, 1076–1079 (1982).
- [2] G. Martinelli and C.T. Sachrajda, “A lattice calculation of the pion’s form factor and structure function,” *Nuclear Physics B* **306**, 865–889 (1988).
- [3] H. R. Fiebig, W. Wilcox, and R. M. Woloshyn, “A Study of Hadron Electric Polarizability in Quenched Lattice QCD,” *Nucl. Phys. B* **324**, 47–66 (1989).
- [4] Matthias Burkardt, Derek B. Leinweber, and Xuemin Jin, “Background-field formalism in nonperturbative QCD,” *Physics Letters B* **385**, 52–56 (1996).
- [5] Andrei Alexandru and Frank X. Lee, “The Background field method on the lattice,” *PoS LATTICE2008*, 145 (2008), [arXiv:0810.2833 \[hep-lat\]](#).
- [6] F. X. Lee, R. Kelly, L. Zhou, and W. Wilcox, “Baryon magnetic moments in the background field method,” *Phys. Lett. B* **627**, 71–76 (2005), [arXiv:hep-lat/0509067](#).
- [7] Frank X. Lee, Leming Zhou, Walter Wilcox, and Joseph C. Christensen, “Magnetic polarizability of hadrons from lattice QCD in the background field method,” *Phys. Rev. D* **73**, 034503 (2006), [arXiv:hep-lat/0509065](#).
- [8] Michael Engelhardt, “Neutron electric polarizability from unquenched lattice QCD using the background field approach,” *Phys. Rev. D* **76**, 114502 (2007), [arXiv:0706.3919 \[hep-lat\]](#).
- [9] Brian C. Tiburzi, “Hadrons in Strong Electric and Magnetic Fields,” *Nucl. Phys. A* **814**, 74–108 (2008), [arXiv:0808.3965 \[hep-ph\]](#).
- [10] W. Detmold, B. C. Tiburzi, and A. Walker-Loud, “Electromagnetic and spin polarizabilities in lattice QCD,” *Physical Review D* **73** (2006), [10.1103/physrevd.73.114505](#).
- [11] W. Detmold, B. C. Tiburzi, and A. Walker-Loud, “Extracting electric polarizabilities from lattice QCD,” *Physical Review D* **79** (2009), [10.1103/physrevd.79.094505](#).
- [12] William Detmold, Brian C. Tiburzi, and Andre Walker-Loud, “Lattice QCD in Background Fields,” *Proceedings, 10th Workshop on Non-Perturbative Quantum Chromodynamics : Paris, France, June 8-12, 2009*, (2009), [arXiv:0908.3626 \[hep-lat\]](#).
- [13] W. Detmold, B. C. Tiburzi, and A. Walker-Loud, “Extracting Nucleon Magnetic Moments and Electric Polarizabilities from Lattice QCD in Background Electric Fields,” *Phys. Rev.* **D81**, 054502 (2010), [arXiv:1001.1131 \[hep-lat\]](#).
- [14] Walter Freeman, Andrei Alexandru, Frank X. Lee, and Mike Lujan, “Update on the Sea Contributions to Hadron Electric Polarizabilities through Reweighting,” in *31st International Symposium on Lattice Field Theory* (2013) [arXiv:1310.4426 \[hep-lat\]](#).
- [15] Michael Lujan, Andrei Alexandru, Walter Freeman, and Frank Lee, “Electric polarizability of neutral hadrons from dynamical lattice QCD ensembles,” *Phys. Rev.* **D89**, 074506 (2014), [arXiv:1402.3025 \[hep-lat\]](#).
- [16] Walter Freeman, Andrei Alexandru, Michael Lujan, and Frank X. Lee, “Sea quark contributions to the electric polarizability of hadrons,” *Phys. Rev. D* **90**, 054507 (2014), [arXiv:1407.2687 \[hep-lat\]](#).
- [17] M. Lujan, A. Alexandru, W. Freeman, and F. X. Lee, “Finite volume effects on the electric polarizability of neutral hadrons in lattice QCD,” *Phys. Rev.* **D94**, 074506 (2016), [arXiv:1606.07928 \[hep-lat\]](#).
- [18] Thomas Primer, Waseem Kamleh, Derek Leinweber, and Matthias Burkardt, “Magnetic properties of the nucleon in a uniform background field,” *Physical Review D* **89** (2014), [10.1103/physrevd.89.034508](#).
- [19] E.V. Luschevskaya, O.E. Solovjeva, O.A. Kochetkov, and O.V. Teryaev, “Magnetic polarizabilities of light mesons in $su(3)$ lattice gauge theory,” *Nuclear Physics B* **898**, 627–643 (2015).
- [20] E. V. Luschevskaya, O. E. Solovjeva, and O. V. Teryaev, “Magnetic polarizability of pion,” *Phys. Lett. B* **761**, 393–398 (2016), [arXiv:1511.09316 \[hep-lat\]](#).
- [21] E. V. Luschevskaya, O. E. Solovjeva, and O. V. Teryaev, “Determination of the properties of vector mesons in external magnetic field by Quenched $SU(3)$ Lattice QCD,” *JHEP* **09**, 142 (2017), [arXiv:1608.03472 \[hep-lat\]](#).
- [22] Emmanuel Chang, William Detmold, Kostas Orginos, Assumpta Parreno, Martin J. Savage, Brian C. Tiburzi, and Silas R. Beane (NPLQCD), “Magnetic structure of light nuclei from lattice QCD,” *Phys. Rev. D* **92**, 114502 (2015), [arXiv:1506.05518 \[hep-lat\]](#).
- [23] Assumpta Parreno, Martin J. Savage, Brian C. Tiburzi, Jonas Wilhelm, Emmanuel Chang, William Detmold, and Kostas Orginos, “Octet baryon magnetic moments from lattice QCD: Approaching experiment from a three-flavor symmetric point,” *Phys. Rev. D* **95**, 114513 (2017), [arXiv:1609.03985 \[hep-lat\]](#).
- [24] Gunnar S. Bali, Bastian B. Brandt, Gergely Endrödi, and Benjamin Gläsel, “Meson masses in electromagnetic fields with Wilson fermions,” *Phys. Rev. D* **97**, 034505 (2018), [arXiv:1707.05600 \[hep-lat\]](#).
- [25] F. Bruckmann, G. Endrodi, M. Giordano, S. D. Katz, T. G. Kovacs, F. Pittler, and J. Wellenhofer, “Landau levels in QCD,” *Phys. Rev. D* **96**, 074506 (2017), [arXiv:1705.10210 \[hep-lat\]](#).
- [26] Amol Deshmukh and Brian C. Tiburzi, “Octet Baryons in Large Magnetic Fields,” *Phys. Rev. D* **97**, 014006 (2018), [arXiv:1709.04997 \[hep-ph\]](#).
- [27] Ryan Bignell, Jonathan Hall, Waseem Kamleh, Derek Leinweber, and Matthias Burkardt, “Neutron magnetic polarizability with Landau mode operators,” *Physical Review D* **98** (2018), [10.1103/physrevd.98.034504](#).
- [28] Ryan Bignell, Waseem Kamleh, and Derek Leinweber, “Pion in a uniform background magnetic field with clover fermions,” *Physical Review D* **100** (2019), [10.1103/physrevd.100.114518](#).
- [29] Ryan Bignell, Waseem Kamleh, and Derek Leinweber, “Pion magnetic polarizability using the background field method,” *Physics Letters B* **811**, 135853 (2020).
- [30] Ryan Bignell, Waseem Kamleh, and Derek Leinweber, “Magnetic polarizability of the nucleon using a Laplacian mode projection,” *Phys. Rev. D* **101**, 094502 (2020), [arXiv:2002.07915 \[hep-lat\]](#).
- [31] Fangcheng He, Derek B. Leinweber, Anthony W. Thomas, and Ping Wang, “Chiral extrapolation of

- the charged-pion magnetic polarizability with Padé approximant,” (2021), [arXiv:2104.09963 \[nucl-th\]](#).
- [32] Hossein Niyazi, Andrei Alexandru, Frank X. Lee, and Michael Lujan, “Charged pion electric polarizability from lattice qcd,” (2021), [arXiv:2105.06906 \[hep-lat\]](#).
- [33] M. Burkardt, J.M. Grandy, and J.W. Negele, “Calculation and interpretation of hadron correlation functions in lattice qcd,” *Annals of Physics* **238**, 441–472 (1995).
- [34] William Andersen and Walter Wilcox, “Lattice charge overlap. 1. Elastic limit of pi and rho mesons,” *Annals Phys.* **255**, 34–59 (1997), [arXiv:hep-lat/9502015](#).
- [35] Walter Wilcox, “Lattice charge overlap. 2: Aspects of charged pion polarizability,” *Annals Phys.* **255**, 60–74 (1997), [arXiv:hep-lat/9606019](#).
- [36] Walter Wilcox and Frank X. Lee, “Towards charged hadron polarizabilities from four-point functions in lattice QCD,” *Phys. Rev. D* **104**, 034506 (2021), [arXiv:2106.02557 \[hep-lat\]](#).
- [37] Frank X. Lee, Andrei Alexandru, Chris Culver, and Walter Wilcox, “Charged pion electric polarizability from four-point functions in lattice QCD,” *Phys. Rev. D* **108**, 014512 (2023), [arXiv:2301.05200 \[hep-lat\]](#).
- [38] Xu Feng, Taku Izubuchi, Luchang Jin, and Maarten Golterman, “Pion electric polarizabilities from lattice QCD,” *PoS LATTICE2021*, 362 (2022), [arXiv:2201.01396 \[hep-lat\]](#).
- [39] X.H. Wang, X. Feng, and L.C. Jin, “Lattice QCD calculation of the proton electromagnetic polarizability,” (2022).
- [40] Murray Moinester, “Pion Polarizability 2022 Status Report,” (2022) [arXiv:2205.09954 \[hep-ph\]](#).
- [41] Murray Moinester and Stefan Scherer, “Compton Scattering off Pions and Electromagnetic Polarizabilities,” *Int. J. Mod. Phys. A* **34**, 1930008 (2019), [arXiv:1905.05640 \[hep-ph\]](#).
- [42] Michael Engelhardt, “Exploration of the electric spin polarizability of the neutron in lattice QCD,” *PoS LATTICE2011*, 153 (2011), [arXiv:1111.3686 \[hep-lat\]](#).
- [43] S. Cabasino et al, “beta=6.0 quenched wilson fermions,” *Physics Letters B* **258**, 195–201 (1991).
- [44] J. Gasser, M.A. Ivanov, and M.E. Sainio, “Revisiting gamma + gamma to pi+ and pi- at low energies,” *Nuclear Physics B* **745**, 84–108 (2006).
- [45] U Bürgi, “Pion polarizabilities and charged pion-pair production to two loops,” *Nuclear Physics B* **479**, 392–426 (1996).
- [46] R. L. Workman and Others (Particle Data Group), “Review of Particle Physics,” *PTEP* **2022**, 083C01 (2022).
- [47] A.M. Baldin, “Polarizability of nucleons,” *Nuclear Physics* **18**, 310–317 (1960).

Appendix A: Magnetic correlation functions

A detailed formalism and notation has been laid out in the study of electric polarizability [37]. Here we present essential equations needed for magnetic polarizability and point out subtle differences.

Eq.(3) is a normalized four-point function where the normalization constant is taken as the wall-to-wall two-point function,

$$\sum_{\mathbf{x}_3, \mathbf{x}_0} \langle \Omega | \psi(\mathbf{x}_3) \psi^\dagger(\mathbf{x}_0) | \Omega \rangle = \text{Tr}_{s,c} \left[\left(\mathcal{W}^T P(t_3) V_{a1}^{(d)} \right)^\dagger \left(\mathcal{W}^T P(t_3) V_{a1}^{(u)} \right) \right] = \text{Tr}_{s,c} \left[\left(\mathcal{W}^T P(t_0) V_{a2}^{(u)} \right)^\dagger \left(\mathcal{W}^T P(t_0) V_{a2}^{(d)} \right) \right]. \quad (\text{A1})$$

Here V_{a1} and V_{a2} are zero-momentum quark propagators emanating from the walls at t_0 and t_3 , respectively,

$$V_{a1}^{(q)} \equiv M_q^{-1} P(t_0)^T \mathcal{W}, \quad V_{a2}^{(q)} \equiv M_q^{-1} P(t_3)^T \mathcal{W}. \quad (\text{A2})$$

Here M_q^{-1} is the inverse quark matrix, $P(t)$ a projector that projects a quark propagator from a given source to time slice t , and \mathcal{W} the wall source.

For diagram a, the unnormalized four-point function with local current (denoted as PC) is written as,

$$\tilde{Q}_{11}^{(a,PC)}(\mathbf{q}, t_1, t_2) = -\frac{4}{9} Z_V^2 \kappa^2 \text{Tr}_{s,c} \left[\left([P(t_2) V_{a2}]^\dagger \gamma_5 \gamma_1 e^{i\mathbf{q}} P(t_2) V_{a1} \right)^\dagger \left([P(t_1) V_{a2}]^\dagger \gamma_5 \gamma_1 e^{i\mathbf{q}} P(t_1) V_{a1} \right) \right]. \quad (\text{A3})$$

Comparing to Q_{44} in the electric case [37], in addition to replacing γ_4 with γ_1 , there is an overall sign change in Q_{11} due to the i factor in j_1^μ in Eq.(5). For conserved current (denoted as PS),

$$\tilde{Q}_{11}^{(a,PS)}(\mathbf{q}, t_1, t_2) = -\frac{4}{9} \kappa^2 \text{Tr}_{s,c} \left[\left([P(t_2) V_{a2}]^\dagger \gamma_5 (1 - \gamma_1) e^{i\mathbf{q}} U_1(t_2, t_2) P(t_2) V_{a1} - [P(t_2) V_{a2}]^\dagger \gamma_5 (1 + \gamma_1) U_1^\dagger(t_2, t_2) e^{i\mathbf{q}} P(t_2) V_{a1} \right)^\dagger \right. \\ \left. \left([P(t_1) V_{a2}]^\dagger \gamma_5 (1 - \gamma_1) e^{i\mathbf{q}} U_1(t_1, t_1) P(t_1) V_{a1} - [P(t_1) V_{a2}]^\dagger \gamma_5 (1 + \gamma_1) U_1^\dagger(t_1, t_1) e^{i\mathbf{q}} P(t_1) V_{a1} \right) \right]. \quad (\text{A4})$$

In our notation, the current split in space is only implicitly carried in the gauge links, not in quark propagators, whereas the split in time is explicitly carried in both the propagators and gauge links. For example, a split at time slice t_2 has the following meaning in the links,

$$\begin{aligned} U_\mu(t_2, t_2 + \hat{\mu}_4) &\equiv \begin{cases} U_4(t_2, t_2 + 1), & \text{if } \mu = 4 \\ U_\mu(t_2, t_2), & \text{if } \mu \neq 4, \end{cases} \\ U_\mu^\dagger(t_2 + \hat{\mu}_4, t_2) &\equiv \begin{cases} U_4^\dagger(t_2 + 1, t_2), & \text{if } \mu = 4 \\ U_\mu^\dagger(t_2, t_2), & \text{if } \mu \neq 4. \end{cases} \end{aligned} \quad (\text{A5})$$

Consequently, U_1 and U_1^\dagger do not commute with $e^{i\mathbf{q}}$, unlike U_4 and U_4^\dagger in the electric case.

For diagram b and local current, we have

$$\tilde{Q}_{11}^{(b,PC)}(\mathbf{q}, t_2) = \frac{5}{9} Z_V^2 \kappa^2 \text{Tr}_{s,c} \left[\left[P(t_2) \gamma_5 V_{a3}^{(1,PC)}(\mathbf{q}) \right]^\dagger \gamma_1 e^{-i\mathbf{q}} P(t_2) V_{a2} \mathcal{W}^T P(t_3) \gamma_5 V_{a1} \right], \quad (\text{A6})$$

where $V_{a3}^{(1,PC)}$ is a SST quark propagator built from V_{a1} ,

$$V_{a3}^{(1,PC)}(\mathbf{q}) \equiv M_q^{-1} P(t_1)^T [\gamma_1 e^{-i\mathbf{q}} P(t_1) V_{a1}]. \quad (\text{A7})$$

Here SST stands for *Sequential Source Technique* which takes an existing quark propagator as the source for a new quark propagator.

For diagram b and conserved current,

$$\tilde{Q}_{11}^{(b,PS)}(\mathbf{q}, t_2) = \frac{5}{9} \kappa^2 \text{Tr}_{s,c} \left[\left[P(t_2) \gamma_5 V_{a3}^{(1,PS)}(\mathbf{q}) \right]^\dagger [(1 - \gamma_1) e^{-i\mathbf{q}} U_1(t_2, t_2) - (1 + \gamma_1) U_1^\dagger(t_2, t_2) e^{-i\mathbf{q}}] P(t_2) V_{a2} \mathcal{W}^T P(t_3) \gamma_5 V_{a1} \right], \quad (\text{A8})$$

where a new inversion is needed for the SST propagator,

$$V_{a3}^{(1,PS)}(\mathbf{q}) \equiv M_q^{-1} \left[P^T(t_1) (1 - \gamma_1) e^{-i\mathbf{q}} U_1(t_1, t_1) P(t_1) V_{a1} - P^T(t_1) (1 + \gamma_1) U_1^\dagger(t_1, t_1) e^{-i\mathbf{q}} P(t_1) V_{a1} \right]. \quad (\text{A9})$$

For diagram c and local current, we have

$$\tilde{Q}_{11}^{(c,PC)}(\mathbf{q}, t_2) = -\frac{5}{9} Z_V^2 \kappa^2 \text{Tr}_{s,c} \left[\left[\gamma_1 e^{i\mathbf{q}} P(t_2) \gamma_5 V_{a1} \right]^\dagger P(t_2) V_{a4}^{(1,PC)}(\mathbf{q}) \mathcal{W}^T P(t_3) \gamma_5 V_{a1} \right]. \quad (\text{A10})$$

where $V_{a4}^{(1,PC)}$ a SST quark propagator built from V_{a2} ,

$$V_{a4}^{(1,PC)}(\mathbf{q}) \equiv M_q^{-1} P(t_1)^T [\gamma_1 e^{i\mathbf{q}} P(t_1) V_{a2}]. \quad (\text{A11})$$

For diagram c and conserved current,

$$\tilde{Q}_{11}^{(c,PS)}(\mathbf{q}, t_2) = -\frac{5}{9} \kappa^2 \text{Tr}_{s,c} \left[\left[P(t_2) \gamma_5 V_{a1}(\mathbf{q}) \right]^\dagger [(1 - \gamma_1) e^{-i\mathbf{q}} U_1(t_2, t_2) - (1 + \gamma_1) U_1^\dagger(t_2, t_2) e^{-i\mathbf{q}}] P(t_2) V_{a4}^{(1,PS)} \mathcal{W}^T P(t_3) \gamma_5 V_{a1} \right], \quad (\text{A12})$$

where

$$V_{a4}^{(1,PS)}(\mathbf{q}) \equiv M_q^{-1} \left[P^T(t_1) (1 - \gamma_1) e^{i\mathbf{q}} U_1(t_1, t_1) P(t_1) V_{a2} - P(t_1)^T (1 + \gamma_1) U_1^\dagger(t_1, t_1) e^{i\mathbf{q}} P(t_1) V_{a2} \right]. \quad (\text{A13})$$